Optics with Imperfect Mirrors
Part II Computational Project

29th April 2019

Abstract

Write fancy abstract here TODO.

---

1 Introduction

Modern telescopes use very finely polished curved mirrors to create sharp images. However, errors are an inherent property of any physical system and any manufacturing process. Thus, regardless of the way mirrors are manufactured (e.g. spin-casting or polishing), there are still imperfections in their shape.

The aim of this paper is a computational investigation of the effects of imperfections in the shape of a telescope mirror on the image. Several relationships are studied, as suggested in the projects manual [1]:

- the effects of tapered illumination on the size and central intensity of the image.
- the effect of a central hole in the mirror, due to the secondary mirror.
- the effects of random and correlated phase errors, due to physical dents in the surface of the mirror. The dents cause phase errors due to the change in path length with respect to the smooth shape.

A more detailed analysis of the theory and techniques used is given in Section 2. Implementation details are discussed in Section 3, and results are presented and discussed in Section 4.

2 Analysis

In the analysis of this problem, we treat the far-field diffraction pattern of the mirror under uniform or Gaussian illumination. In the far field regime, the diffraction pattern of an aperture is given by the Fourier Transform of the aperture function $A(x, y)$ [3, Chapter 10.2]. This is a reasonable approximation as long as:

$$\frac{R^2}{\lambda D} \ll 1, \tag{1}$$

known as the Fraunhofer limit, where R is the maximum extent of the aperture, λ is the wavelength of radiation and D is the distance from the aperture to the screen onto which the image is projected. In this problem we use:

$$\lambda = 1\,\text{mm}$$
$$R = 6\,\text{m},$$

which would require a distance on the order of 1 km for the far-field limit to hold.

However, considering parabolic mirrors brings the image plane closer. Besides, we can work in angular coordinates, with the image space spanned by:

$$p = k \sin\theta \approx \frac{kx'}{D}$$
$$q = k \sin\chi \approx \frac{ky'}{D},$$

where x' and y' are distances that would span a physical image plane, and k is the wavenumber. We thus eliminate the dependence on D. In these coordinates, the diffraction pattern is:

$$\psi(p,q) \propto \iint A(x,y) \exp\left(ipx + iqy\right) dxdy, \tag{2}$$

which is just a Fourier transform of A. In the figures of diffraction patterns I produce, the axes will be p and q.

NB: Seemingly we've also eliminated the dependence on λ, but that will be needed again in the analysis of dented mirrors (Section 2.5).

What is the meaning of this diffraction pattern? Since the incoming light is multiplied by the telescope's aperture function, the resulting image is a convolution of the astronomical objects being observed and the diffraction pattern of $A(x,y)$. Intuitively, for point-like stars, they will be seen through the telescope as "copies" of the diffraction pattern. Two factors are thus crucial:

- The width of the central disk, which limits the resolution of the telescope. If two objects are closer than this central width, they cannot be resolved [3, Section 10.2.6].
- The central intensity, which sets a lower bound on the brightness of objects that can be observed.

2.1 Discrete Fourier Transforms

The fact that the image is a Fourier transform of the aperture function is very useful. Fast Fourier Transform algorithms can compute discrete Fourier transforms of multi-dimensional data efficiently, and there exist many library implementations thereof. Here, the C++ `FFTW 3` library [2] was chosen, as suggested in the projects manual [1]. It is a well-established and well-tested library with very good computational efficiency.

Minor adaptations are required to use the DFT algorithms in the library. The 1D discrete Fourier transform is defined as [4, Chapter 12.1]:

$$H_k \propto \sum_{n=0}^{N-1} h_n \ \exp\left\{\left(2\pi i \frac{kn}{N}\right)\right\}, \tag{3}$$

with the corresponding frequency values:

$$f_k = \frac{k}{N\Delta}, \quad k = 0..N-1, \tag{4}$$

where Δ is the sampling interval of the original signal. Comparing to a 1D discrete form of the diffraction integral (Equation 2):

$$\psi_k \propto \sum_{n=0}^{N-1} A_n \exp\{(ip_k x_n)\}, \quad \text{where} \quad x_n = n\Delta \tag{5}$$

we see that we need to rescale:

$$p_k = 2\pi f_k. \tag{6}$$

2.2 Testing

To determine whether the program is outputting something sensible, we need to test it on a range of known results. Diffraction patterns for the following kinds of apertures are easy to compute analytically, and thus can be used for testing the program.

Rectangular aperture A rectangular aperture of size $-a < x < a$, $-b < y < b$ has diffraction pattern:

$$\psi(p,q) \propto \frac{\sin(pa)}{pa} \frac{\sin(qb)}{qb}, \tag{7}$$

thus it's expected to have the first zeros at:

$$p = \pm\frac{\pi}{a} \quad \text{and} \quad q = \pm\frac{\pi}{b}. \tag{8}$$

Circular aperture A circular aperture of radius R has a diffraction pattern called an Airy disc, with angular radius:

$$\sin\theta \approx 1.22\frac{\lambda}{2R} \quad \Rightarrow \quad p = 1.22\frac{\pi}{R}. \tag{9}$$

Both of these minima should appear in the diffraction patterns, and the scaling with the inverse of the aperture size should be observable.

2.3 Tapered aperture function

The amplitude of light illuminating a telescope mirror is often not uniform. A "taper" or "grading" is chosen, usually in the form of a Gaussian curve [6, Section 6.4]:

$$A(r) = \begin{cases} e^{-r^2/2\sigma^2} & ,r \le R \\ 0 & ,r > R \end{cases}, \quad \text{where} \quad r^2 = x^2 + y^2. \tag{10}$$

This is the multiplication of a Gaussian with a circular aperture of radius R. From the convolution theorem, its diffraction pattern is the convolution between another Gaussian and a Bessel function. Intuitively, this should lead to a "smearing" of the central maximum relative to a uniformly-lit mirror. Since the variance of a Gaussian is inversely proportional to the variance of its F.T., the smearing will be stronger at small σ.

Therefore, at small σ, the full width at half power (FWHP) should follow:

$$\Delta p_{\text{hp}} \propto \sigma^{-1}. \tag{11}$$

At large σ, as A approaches uniform illumination, the image tends to a Bessel function, and the FWHP will approach a constant value. Besides, since at smaller σ the integral of $|A|$ over the aperture is smaller, the central intensity should be smaller, tending to 0 as $\sigma \to 0$.

While the taper widens the central maximum, it also leads to suppression of the side lobes of the Airy pattern, thus possibly improving the resolution. See [3, Section 11.3] for an explanation.

2.4 Central hole

Classical telescopes, such as the Cassegrain design, have a central hole in the primary mirror due to the secondary mirror [6, Section 7.2.3]. The resulting aperture function can be viewed as the difference between that of the complete mirror (A_{complete}) and that of the hole (A_{hole}). Due to the linearity of the Fourier Transform, the diffraction pattern of this mirror should be the difference between the patterns of A_{complete} and A_{hole}.

We can quantify how similar these results are by subtracting the image produced by a holed aperture from the difference of the images produced by A_{complete} and A_{hole}.

Due to the Airy disc of the smaller A_{hole} being larger than that of the complete mirror, we expect the entire central disc to be dimmer due to the hole. The secondary rings should become irregular, because they have different frequencies in the patterns of A_{complete} and A_{hole}.

2.5 Bent mirrors

Mirror surfaces could have deformations in them due to manufacturing errors, altering the phase of light. As seen in Figure 1, the effect is that, for a dent of depth ε, there is a path difference of 2ε, leading to a phase difference of:

$$\Delta\varphi = 2k\varepsilon = \frac{4\pi}{\lambda}\varepsilon \tag{12}$$

We are going to investigate the effect of two types of phase errors:

- without spatial correlation, with a given RMS
- spatially correlated, to simulate bends in the mirror.

The expected effect of these errors is to decrease the central intensity of the image, as they introduce decoherence to the light.

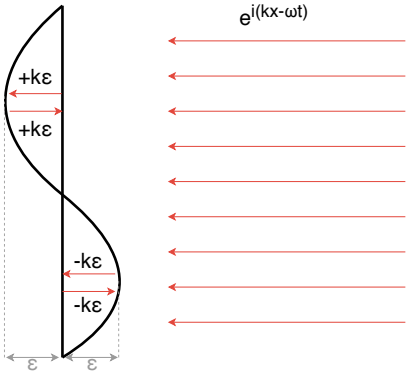

Figure 1: effect of deformations in the mirror surface on the phase of the wave. A deformation of depth ε produces an optical path difference of 2ε, one for the incident wave and one for the reflected wave.

3 Implementation

The implementation consists of several different parts, discussed in the subsections that follow. The overall logic flow of the program is: The executable is invoked with one argument, pointing to a configuration file. The instructions therein are read and executed in order, thus computing diffraction patterns for the described apertures. The results are printed to disk, and figures can then be produced by invoking the respective Python scripts for each problem.

C++ source files are in `src/cpp`, and plotting scripts in `src/scripts`. Data is written by convention to the `data` directory, and figures to `fig`.

3.1 Describing Apertures and Images

In the `FFTW` library two-dimensional N_x by N_y arrays are represented as one-dimensional arrays of complex numbers (the inbuilt `complex` type [5]) of length $N_x \times N_y$ [2, Section 3.2].

Because working directly with a 1D representation of 2D data can be clunky, I decided to wrap this functionality in a class called `Array2d`, declared in the header with the same name. The class stores the data internally in the 1D array representation, but has a more user-friendly interface. It defines the `[i][j]` and `(i, j)` operators for easy access to the element in the i^{th} row and j^{th} column.

FFTW compatibility The method `ptr()` returns a pointer to the beginning of the array, cast to `fftw_complex` type. This pointer can be passed to functions in the `FFTW` library [2, Section 4].

Memory allocation One special feature of this class that breaks with convention is that the (compiler generated) copy constructor only performs a shallow copy, copying the pointer to the data array, but not the data itself. Only the explicitly defined constructor `Array2d::Array2d(int nx, int ny)` uses `fftw_alloc_complex` to allocate new memory for the array. This means that the user of the class has finer control over where memory is allocated, which is important in the case of large arrays. For example, using IEEE double-precision floating point, which occupies 64 bits of memory, a $2^{13} \times 2^{13}$ array of complex numbers occupies around 1 GB of memory.

For better understanding of when memory is allocated, compile the code with the variable `DEBUG_OUT` set to `true` in `array2d.cpp`. Then the calls to the constructor and destructor of `Array2d` will be printed to console.

Aperture generators These are a type of function that initialise an `Array2d` with a particular kind of aperture with given parameters. For example, there is a generator for circular apertures, one for circular Gaussian-illuminated, one for circular with random errors, etc.

3.2 Configuration Files

Configuration files are stored by convention in the `config` directory, and are a series of `key = value` lines. They contain:

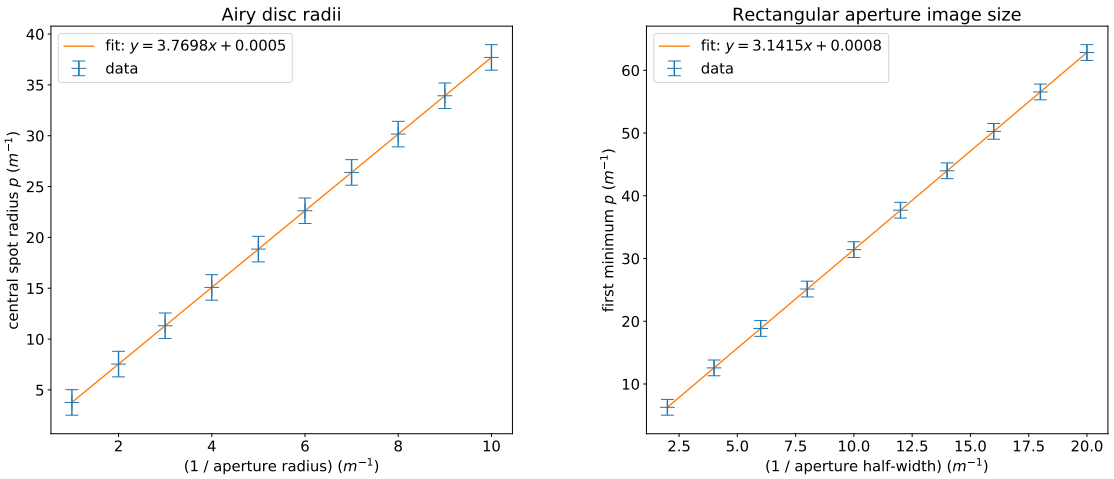

(a) (b)

Figure 2: Sizes of central spots as function of aperture size, for both round and rectangular apertures.

- `nx` and `ny`. These are the size of input and output arrays.
- `tasks`, what actions to perform on each of the shapes
- `n_shapes`, the number of shapes
- for each shape, its properties: `type` (the name of the aperture generator), `lx` and `ly` (the domain of $A(x, y)$), and `params`, a list of parameters of the shape, e.g. the dimensions or the taper of Gaussian illumination.

3.3 The `fftshift` operation

The result of this operation is shifting the zero-frequency component of the spectrum from the beginning to the middle of an array. This takes advantage of the fact that the Fourier frequencies (Equation 4) are cyclic with period $1/\Delta$ [4, Section 12.1.2]. Applying this is required to see a diffraction pattern as it would appear on a screen.

3.4 Correlating errors

As mentioned in Section 2.5, we want to investigate the effects of spatially-correlated phase errors. To produce such deformations, we convolve random gaussian-distributed numbers with a gaussian shape of the desired correlation width, as suggested in the manual [1]. Taking advantage of the convolution theorem, this is equivalent to multiplication of FTs of the two shapes, followed by a reverse FT. The numbers are then normalised to the desired RMS and set as the phase in the "mirror" array. The `corr_errors` aperture generator implements this.

We want to ensure that the phase error produced by this method is the desired one, and that it doesn't change with the correlation length l_c. These properties are tested in Section 4.5.

4 Results and Discussion

4.1 Tests

First, I ran the program on series of circular and rectangular apertures described in `config/circular_mins.txt` and `config/rectangle_mins.txt`, expecting to see a linear relationship between the extent of the central maximum and the inverse of the aperture size (see Section 2.2). As seen in Figure 2, these

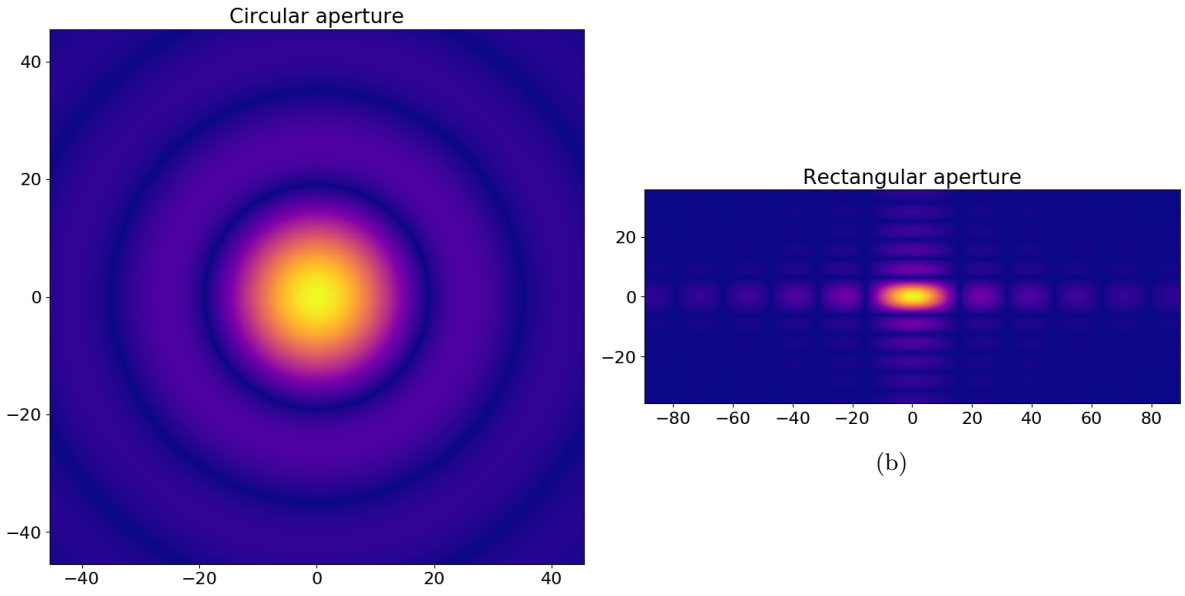

(a) (b)

Figure 3: Typical diffraction patterns of circular and vertical rectangular apertures.

linear relationships hold. The line slopes are close to the expected values of 1.22π for the Airy disc and π for rectangular shapes.

Figure 3 shows that the diffraction patterns look as expected. Most notably, the image from a vertical rectangle is longer along the horizontal axis, as expected from Equation 8.

4.2 Gaussian Illumination

Figure 4 shows the results anticipated in Section 2.3, especially the low and high σ limits. At low σ, the FWHM $\propto 1/\sigma$, and the central intensity tends to zero. At high σ, both properties approach their uniform illumination values:

$$\text{FWHP} \to (0.641 \pm 0.014)\,\text{m}^{-1}$$
$$I(0,0) \to\sim 30 \times 10^3.$$

These results support the expected behaviour of Gaussian-illuminated apertures. Note that the shape in Figure 4b is inherently hard to quantify since it results from the integral of a Gaussian, which has no analytical form.

Figure 5 shows the images produced by illuminating the same mirror uniformly or with a taper. The uniformly lit mirror produces much sharper secondary rings. This suggests that the reason for using a taper is to concentrate more of the power in the central spot, and avoid the effects of the secondary peaks on image quality.

4.3 Central hole

Figure 6 shows the results of the calculation suggested in Section 2.4. We can see the amplitude of the difference reaching at most around 2×10^{-5}. In the original diffraction patterns, the central amplitude is on the order of 10^4, so indeed the two patterns are equal to a very high accuracy. The differences are on the order of the precision to which the numbers were printed before plotting, around 10^{-6}.

This confirms that the F.T. operations we use are linear to a good accuracy.

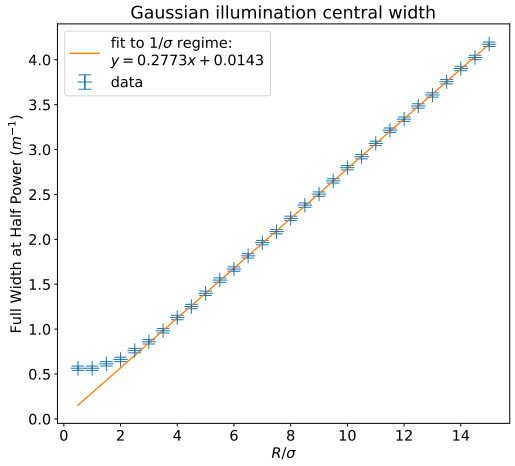

(a) Dependence of full width at half maximum on aperture taper. The fit is for $R/\sigma > 3$.

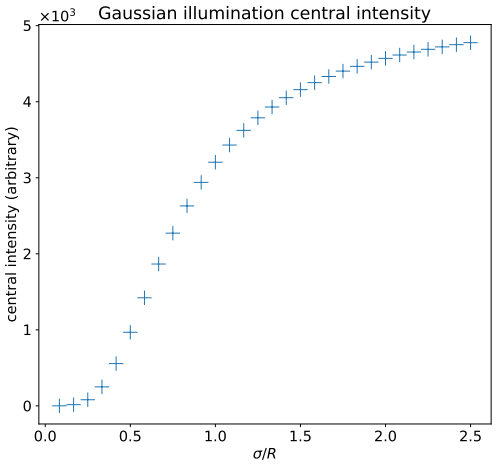

(b) Central intensity variation with aperture taper.

Figure 4: Properties of Gaussian illumination diffraction pattern.

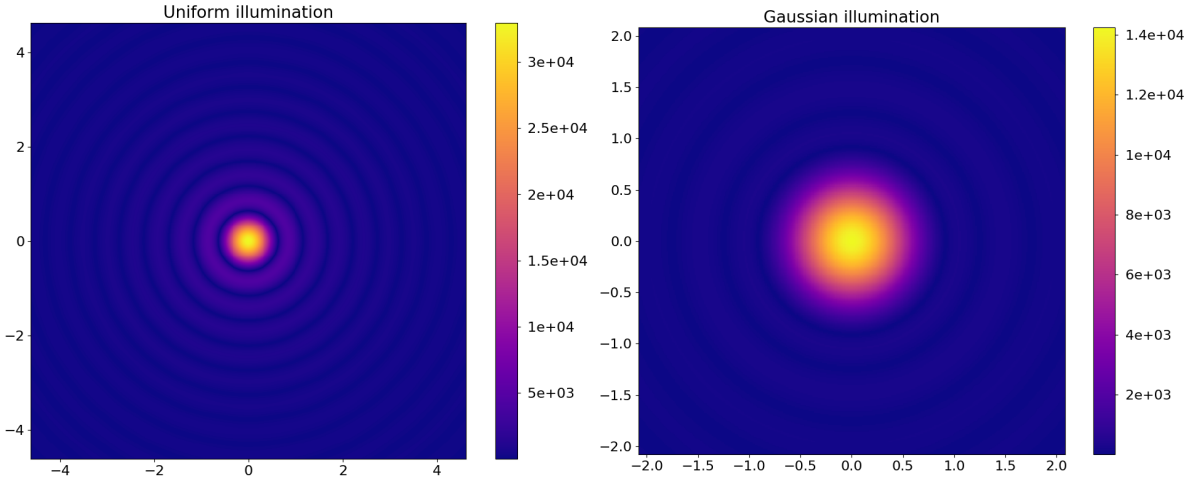

(a) (b)

Figure 5: Amplitude diffraction patterns of two different illumination patterns of the same mirror of radius $R = 6\,\mathrm{m}$. Note the different scales of the images.

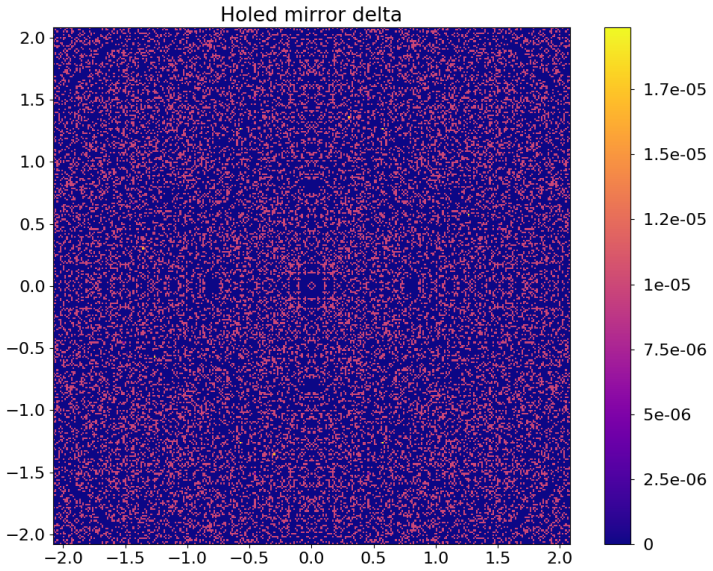

Figure 6: The diffraction pattern of a mirror with a central hole of radius $r = 0.5\,\mathrm{m}$ was subtracted from the difference of diffraction patterns of a complete mirror and just the central hole.

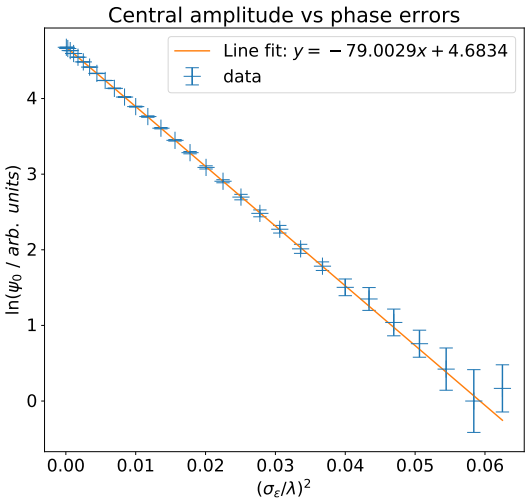

(a) dependence of the central amplitude on the RMS phase (wavefront) error. Note logarithmic scale of the vertical axis.

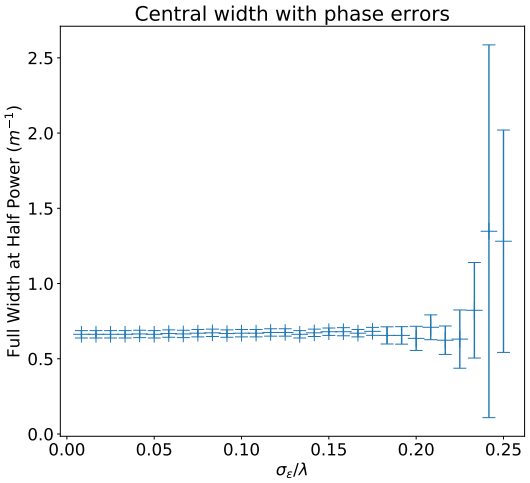

(b) (lack of) relationship of full-width-at-half-power with random phase errors.

Figure 7

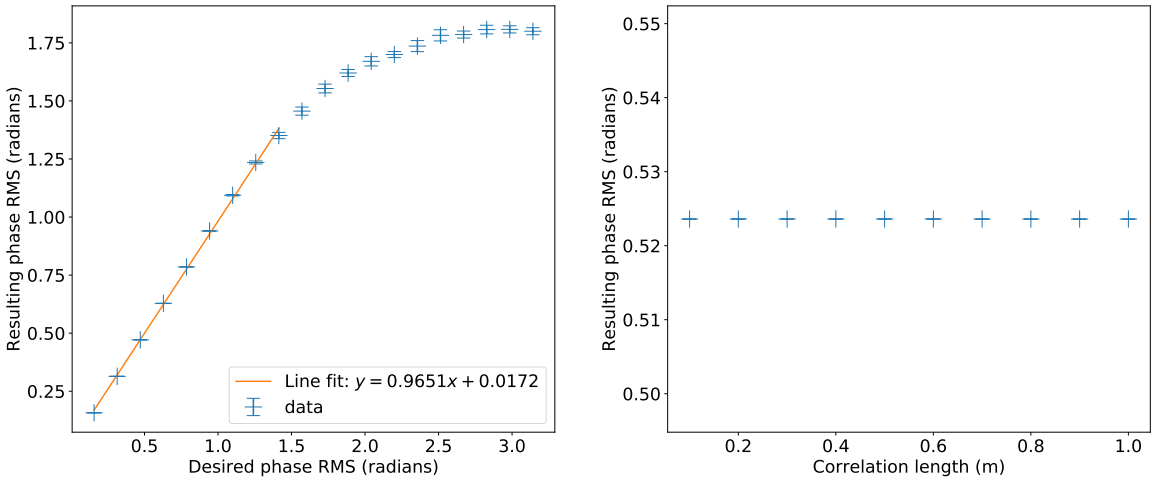

(a) (b)

Figure 8: dependence of RMS (root mean square) phase on desired RMS and correlation length.

4.4 Random errors

Figure 7 shows how properties of the image are affected by random errors. The with of the central disc is unaffected, but the central amplitude (ψ_0) decreases with the RMS error σ_ε. When $\sigma_\varepsilon = \sqrt{\langle \Delta\varphi^2 \rangle} \to \pi$, the amplitude tends to zero. The linear relationship in Fig. 7a indicates that the amplitude is a Gaussian function of the wavefront error:

$$\psi_0 \propto \exp\left(-\frac{(\sigma_\varepsilon/\lambda)^2}{2\sigma_\psi^2}\right), \tag{13}$$

with

$$\sigma_\psi = (79.56 \pm 0.03) \times 10^{-3} \tag{14}$$

given by the line slope.

The implication for telescopes is that larger wavefront errors will decrease the apparent brightness of the observed objects.

4.5 Error correlation tests

In Figure 8a we see that the produced RMS phase error is close to the desired one for phases of up to $\frac{\pi}{2}$. It saturates to about 1.8 rad at larger desired σ_ε, probably due to some numbers falling outside the $(-\pi,\ \pi)$ range, and overflowing when they are converted to complex phase. This is expected behaviour.

In Figure 8b we see that the RMS error does not depend on correlation length, which confirms normalisation is correct.

4.6 Spatially correlated errors

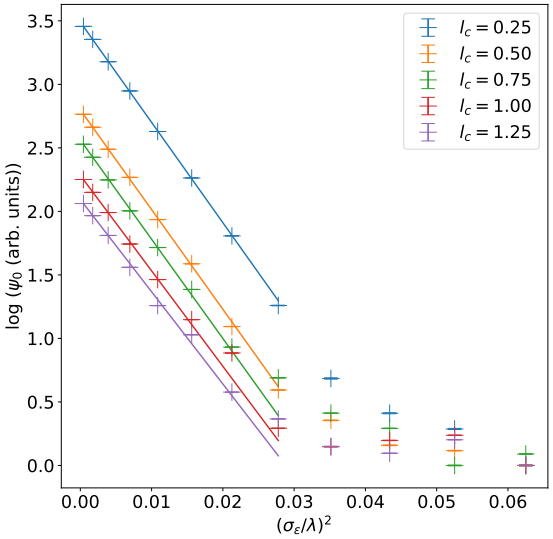

(a) dependence of central amplitude on the RMS of correlated phase errors.

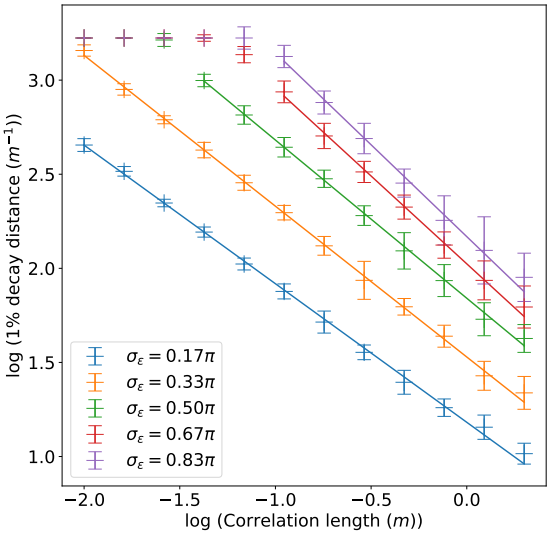

(b) farthest distance from the centre where an amplitude at least 1 m of the central one is found, as a function of error correlation length (or defect 'width').

Figure 9

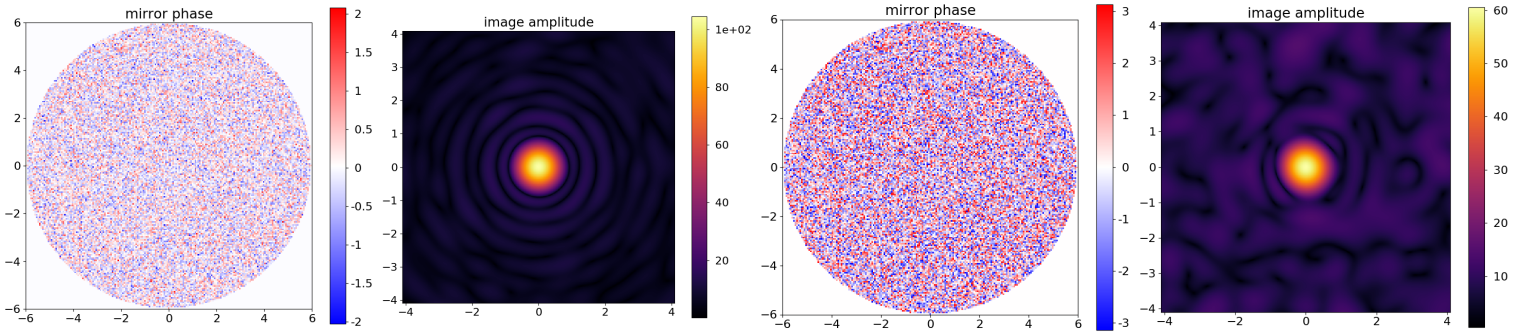

(a) $\sigma_\varepsilon = \pi/6$ (b) $\sigma_\varepsilon = \pi/2$

Figure 10: Typical random error aperture functions and resulting diffraction patterns. Amplitudes are raised to the power 1/2 to make features easier to see.

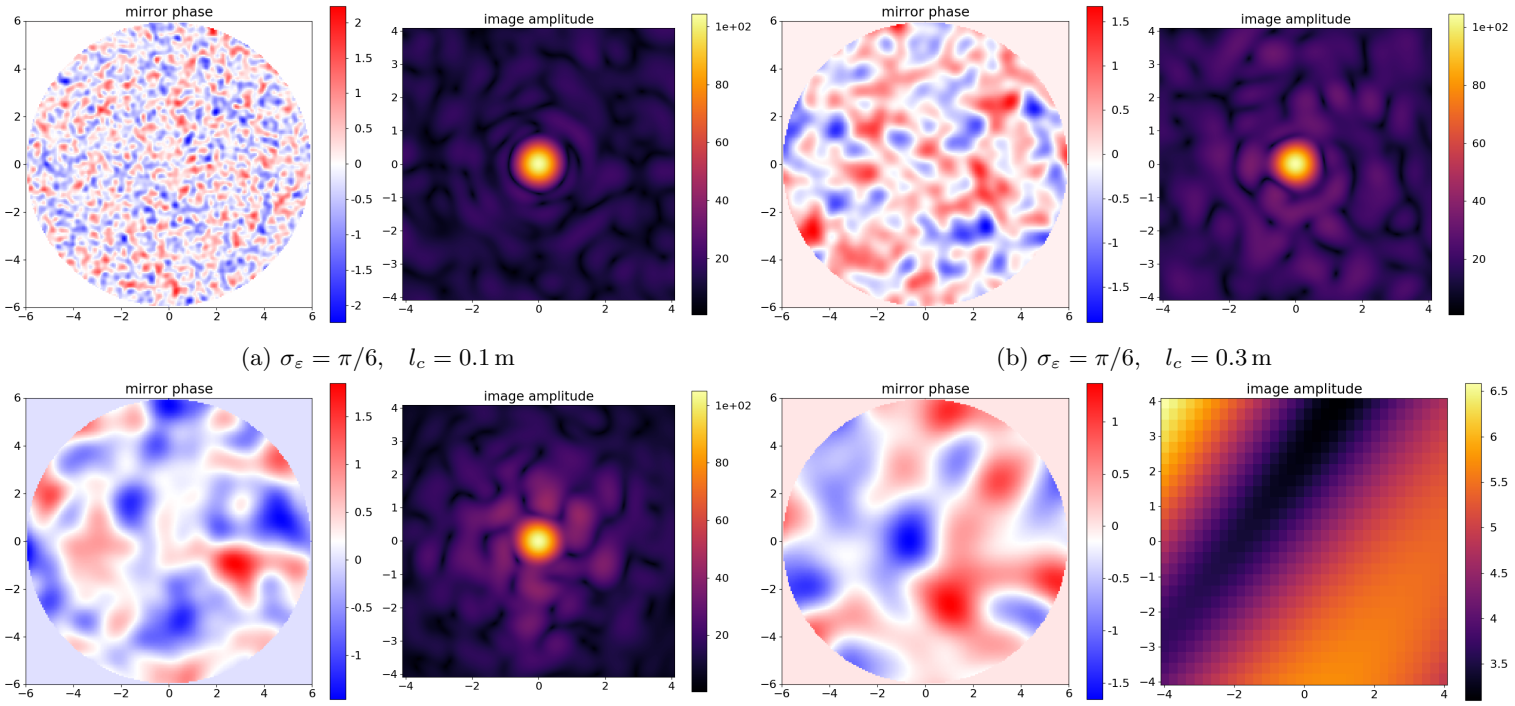

(a) $\sigma_\varepsilon = \pi/6, \quad l_c = 0.1\,\mathrm{m}$ (b) $\sigma_\varepsilon = \pi/6, \quad l_c = 0.3\,\mathrm{m}$

(c) $\sigma_\varepsilon = \pi/6, \quad l_c = 0.5\,\mathrm{m}$ (d) $\sigma_\varepsilon = \pi/6, \quad l_c = 0.8\,\mathrm{m}$

Figure 11: Typical correlated error aperture functions and resulting diffraction patterns. Amplitudes are raised to the power 1/2 to make features easier to see.

5 Conclusion

References

[1] David Buscher. *Part II Computational Physics Projects*. Cavendish Laboratory, University of Cambridge. Lent 2019. URL: https://www-teach.phy.cam.ac.uk/dms/dms_getFile.php?node=20927 (visited on 03/04/2019).

[2] Matteo Frigo and Steven G. Johnson. *FFTW. (version 3.3.8)*. [library documentation]. Massachusetts Institute of Technology. May 2018. URL: http://www.fftw.org/fftw3.pdf (visited on 04/04/2019).

[3] Eugene Hecht. *Optics*. 5th edition. Pearson Education, 2017. ISBN: 978-1-292-09693-3.

[4] William H. Press et al. *Numerical Recipes. The Art of Scientific Computing*. 3rd edition. Cambridge University Press, 2007. ISBN: 9780521880688.

[5] *std::complex*. cppreference. URL: https://en.cppreference.com/w/cpp/numeric/complex (visited on 26/04/2019).

[6] Thomas L. Wilson, Kristen Rohlfs and Susanne Hüttemeister. *Tools of Radio Astronomy*. 5th edition. Berlin Heidelberg: Springer, 2009. ISBN: 978-3-540-85121-9.

A Code listing

A.1 Numerical routines in C++

A.2 Plotting in Python